JOURNAL OF APPLIED SCIENCES RESEARCH

ISSN: 1819-544X EISSN: 1816-157X

JOURNAL home page: http://www.aensiweb.com/JASR 2015 March; 11(4): pages 30-38.

Published Online 28 January 2015. **Research Article**

New Model for Measurements of Light Extinction and Absorption Cross Section Spectra by Nanoparticles

Akbar Asadi

Department of Physics, Maritime University Of Imam Khomaini, Nowshahr, Iran.

Received: 1 January 2015**; Accepted:** 25 January 2015

ABSTRACT

In this paper, a novel dispersion model, referred to as the General Model is proposed for modeling arbitrary linear dispersive materials. This model is proved to be more efficient in fitting the material permittivity functions compared with the conventional Debye, Drude and Lorentz models. A generally applicable method is introduced to estimate the parameters of this model with no initial guess requirement, which makes it feasible in practical applications. The new model is implemented in the FDTD method to improve the efficiency of simulating optical devices in a wide wavelength range. The absorption and extinction cross section spectra characteristics of different nanoparticles are systematically studied by employing the implemented method.

Keywords: General Model**,** FDTD, cross section spectra, nanoparticles**..**

INTRODUCTION

Dispersive materials, such as metals, are widely used in optical devices. TheFinite-Difference Time-Domain (FDTD) method [8]. is one of the most common choices for simulating such devices in a wide frequency range. One of the most important advantages of the FDTD method is that the broadband response can be accurately obtained in only one simulation run [2].Several simple dispersion models, such as multi-pole Debye, Drude, and Lorentz models, have been widely adopted for modeling dispersive materials using the FDTD method [12].To fit permittivity function of a given material accurately in awide frequency range, a large number of poles are required in these models. Rakic and Djurisic used the Durde model with up to five Lorentzian terms to fit the permittivity functions of eleven metals [7]. Hao and Nordlander proposed an improved model consisting of four Lorentzian terms to fit dielectric data of gold. All the proposed multi-pole models archived good fit to the measure data. However, using a dispersion model with a large number of poles not only requires a lot of efforts for modal parameter estimation but also dramatically increases the memory and computational costs of the FDTD method [12].Han, Dutton and Fan [4] proposed a complex-conjugate pole-residue pair model and implemented it in the FDTD method to increase the modeling efficiency [10].However, these authors did not propose an efficient method for the parameters estimation.TheFDTD formulation for dispersive materials are developed using the Z transform and frequency approximation methods [1].In this paper, a dispersion model, referred to as the general model with a parameter estimation method is proposed for the simulation of optical properties of arbitrary linear dispersive media over a wide wavelength range. Theconventional Debye, Drude and Lorentz models are derivable from this general model. The time domain properties of the proposed model are analyzed. It is demonstrated that the model can fit the relative permittivity data of a material accurately and efficiently in a wide wavelength range and the parameters of this model can be estimated requiring no initial guess. Thegeneral model is implemented in the FDTD method as a powerful and computationally efficient

Corresponding Author: Akbar Asadi, Department of Physics, Maritime University Of Imam Khomaini, Nowshahr, Iran.
Tel:+98-66476794; E-mail:Asadi.mui@gmail.com

tool for simulating nanoparticles of dispersive materials in a wide wavelength range of light. By employing this model, a systematic study of the optical properties of different nanoparticles gives a good reference for designs of optical devices utilizing the cross-section spectra characteristics of nanoparticles.

2. General Dispersion Model:

Assuming the time harmonic dependence, $e^{j\omega t}$, the general model is proposed to describe the dispersive material's relative permittivity expressed by the fraction form as

$$\varepsilon_r(\omega)=\frac{\sum_{k=1}^{N} a_k (j\omega)^k}{\sum_{k=1}^{N} b_k (j\omega)^k} \quad (1a)$$

Where a_k, b_k are real numbers. The fraction form is the ratio of two polynomials $\sum_{k=1}^{N} a_k (j\omega)^k$ and $\sum_{k=1}^{N} b_k (j\omega)^k$, where the highest order of the denominator is the same as that of the numerator. To be conveniently adopted by the FDTD method, the general model is represented by its partial fraction expansion described by

$$\varepsilon_r(\omega) = \varepsilon_\infty + \sum_{k=1}^{L} \chi_k(\omega) \quad (1b)$$

Where

$$\chi_k(\omega)=\frac{\sum_{n=0}^{q-2} C_n (j\omega)^n}{\sum_{n=0}^{q} D_n (j\omega)^n} \quad (2a)$$

Where C_k, D_k are real numbers.

Or,

$$\chi_k(\omega) = \begin{cases} \frac{r_k}{j\omega - p_k} & ; \text{ if } p_k \text{ is real} \\ \frac{r_k}{j\omega - p_k} + \frac{r^*_k}{j\omega - p^*_k} & ; \text{ if } p_k \text{ is complex} \\ \sum_{u=1}^{U} \frac{r_{k,u}}{(j\omega - p_k)^u} & ; \text{ if } p_k \text{ is a multiple root} \end{cases} \quad (2b)$$

Where ε_∞, r_k and p_k; are the direct coefficient, residue, and pole, respectively. The partial fraction term $\chi_k(\omega)$, is the frequency domain susceptibility function. It has three forms depending on the properties of the pole p_k: 1) a real fraction term with a real residue and a real pole, when p_k is a real number; 2) two complex fraction terms consist of complex conjugate residue and pole pairs, when p_k is a complex number; and 3) a summation of fraction terms which contains high order (>1) of $j\omega$, when p_k is a multiple root of the denominator $\sum_{K=1}^{N} b_k (j\omega)^k$. It is observed that the third expression of p_k should be avoided in the parameter

It shows that Debye, Drude, and Lorentz models are all special cases of general model with specified parameters. The general model treats the Debye, Drude, and Lorentz materials in a unified.

Table 1: Coefficients of dispersion models**.**

Model	$\varepsilon_r(\omega)$	L	p_k	r_k	p_{k+1}	r_{k+1}
Debye	$\varepsilon_\infty + \sum_{p=1}^{N_p} \frac{\Delta\varepsilon_p}{j\omega\gamma_p + 1}$	N_p	-1/γ_k	$\frac{\Delta\varepsilon_k}{\gamma_k}$	--	--
Drude	$\varepsilon_\infty + \sum_{p=1}^{N_p} \frac{\omega_p^2}{-\omega^2 + j\omega\gamma_p}$	$2N_p$	0	$\frac{\omega_p^2}{\gamma_p}$	$-\gamma_p$	$-\frac{\omega_p^2}{\gamma_p}$
Lorentz	$\varepsilon_\infty + \sum_{p=1}^{N_p} \frac{\Delta\varepsilon_p \omega_p^2}{-\omega^2 + 2j\omega\gamma_p + \omega_p^2}$	N_p	$-\gamma_p - j\sqrt{\omega_p^2 - \gamma_p^2}$	$j\frac{\Delta\varepsilon_p \omega_p^2}{2\sqrt{\omega_p^2 - \gamma_p^2}}$ $(\omega_p > \gamma_p)$	-	-
Complex-conjugate pole- residue pair	$\varepsilon_\infty + \sum_{k=1}^{N_p} (\frac{r_k}{j\omega - p_k} + \frac{r_k^*}{j\omega - p_k^*})$	N_p	Complex number	Complex number	-	-

Formulation, which simplifies the implementation of dispersion models in numerical simulation algorithms, such as the FDTD method. It also shows that when, p_k is a complex number, the partial fraction form of the

General model is the same as the complex conjugate pole-residue pair model.

To study properties of the general model in time domain, the inverse Fourier transformation is performed on the frequency domain susceptibility function $\chi_k(\omega)$ defined in equation (2b). If p_k is a real number, the time domain susceptibility is expressed by

$$\chi_k(t) = r_k e^{p_k t} U(t) \quad (3)$$

Where, U(t) is the unit step function. It shows that when $p_k > 0$, the susceptibility is exponentially growing with time, which contradicts the phenomenon that the lightwave is decaying when propagating in lossymaterials, such as metals. Thus, the parameter p_k should not be greater than zero when modeling lossy materials in this model. If p_k is a complex number, the frequency domain susceptibility can be reformed as

$$\chi_k(\omega) = \frac{(-r_k p_k^* - p_k r_k^*)}{-\omega^2 - (p_k^* + p_k)j\omega + p_k^* p_k} + \frac{(r_k + r_k^*)}{-\omega^2 - (p_k^* + p_k)j\omega + p_k^* p_k} \quad (4)$$

The time domain susceptibility is obtained by taking the inverse Fourier transformation, as expressed by

$$\chi_k(t) = \zeta_k e^{-\alpha_k t} \sin(\kappa_k t) U(t) + \frac{d}{dt}[\xi_k e^{-\alpha_k t} \sin(\kappa_k t) U(t)] \quad (5)$$

Where

$$\alpha_k = \frac{-(p_k^* + p_k)}{2} \kappa_k = \sqrt{p_k^* p_k - \alpha_k^2}$$

$$\zeta_k = \frac{(-r_k p_k^* - p_k r_k^*)}{\kappa_k} \xi_k = \frac{(r_k + r_k^*)}{2}$$

It is noteworthy that when the real part of p_k is positive, the parameter α_k is negative (α_k <0). The time domain susceptibility $\chi_k(t)$will grow exponentially with time, which contradicts the property of the lossy materials. The above analysis comes out a natural conclusion that the real part of the pole parameter $p_k$should not be bigger than zero α_k>0 , when using the general model to model lossy dispersive materials.

The general model can be easily and efficiently implemented in the FDTD method with an auxiliary differential equation (ADE) scheme. In Maxwell's equations, Ampere's law in frequency domain is expressed by

$$j\omega\varepsilon_0\varepsilon_\infty\widetilde{\boldsymbol{E}} + \boldsymbol{\sigma}\widetilde{\boldsymbol{E}} + \sum_{\boldsymbol{k=1}}^{\boldsymbol{L}}\tilde{\boldsymbol{J}}_{\boldsymbol{k}} = \boldsymbol{\nabla}\times\widetilde{\boldsymbol{H}} \qquad (6)$$

Where,$\mathbf{J_k}$is the polarization current related with each term in the summation of the general model, defined by

$$\tilde{\boldsymbol{J}}_{\boldsymbol{k}} = \begin{cases} j\omega\varepsilon_0\widetilde{\boldsymbol{E}}\frac{r_k}{j\omega - p_k}; & \text{if } p_k \text{ is real} \\ j\omega\varepsilon_0\widetilde{\boldsymbol{E}}\left(\frac{r_k}{j\omega - p_k} + \frac{r_k^*}{j\omega - p_k^*}\right); & \text{if } p_k \text{ is complex} \end{cases} \qquad (7)$$

As mentioned previously, the multiple-root $p_k$should be avoided in the parameter estimation procedure, so that it would not be concerned with the difficult implementation of polarization current in the multiple-root$p_k$case. If $p_k$is real, $r_k$is also real. Then the time-domain polarization current is real and given by

$$\frac{\partial \mathbf{J}_k}{\partial t} - p_k\mathbf{J}_k = r_k\varepsilon_0\frac{\partial \boldsymbol{E}}{\partial t} \qquad (8)$$

If $p_k$is complex, $r_k$is also complex. The time-domain polarization current has two parts$\mathbf{J}_k$and $\mathbf{J}_k'$, corresponding to the two complex poles in equation (7). The two polarization currents are all complex and given by

by

$$\frac{\partial \mathbf{J}_k}{\partial t} - p_k\mathbf{J}_k = r_k\varepsilon_0\frac{\partial \boldsymbol{E}}{\partial t} \qquad (9)$$

$$\frac{\partial \mathbf{J}_\mathbf{k}'}{\partial t} - p_k^*\mathbf{J}_\mathbf{k}' = r_p^*\varepsilon_0\frac{\partial \boldsymbol{E}}{\partial t} \qquad (10)$$

Because **E**(t) is real, if the initial values for the two polarization current are the same, the two parts are mutual complex conjugate, i.e.$\mathbf{J}_\mathbf{k}' = \mathbf{J}_\mathbf{k}^*$.Only one complex equation, either equation (9) or (10), needs to be computed in the FDTD calculation. In the following derivation, equation (9) is employed. Therefore, when $p_k$is complex, the real part of the time domain polarization current is Re $[F^{-1}(\tilde{\boldsymbol{J}}_{\boldsymbol{k}})]$=2 Re $(\mathbf{J}_k)$ .By applying the inverse Fourier transform on both sides of equation(6), the time domain Ampere's curl equation is obtained as

$$\varepsilon_0\varepsilon_\infty\frac{\boldsymbol{\partial}}{\boldsymbol{\partial t}}\mathbf{E} + \boldsymbol{\sigma}\mathbf{E} + \sum_{\boldsymbol{k=1}}^{\boldsymbol{L}} mRe(\mathbf{J}_{\boldsymbol{k}}) = \boldsymbol{\nabla}\times\mathbf{H} \qquad (11)$$

Where m =1if $p_k$is real; m = 2 if $p_k$is complex. The time domain polarization current equation and Ampere's curl equation are combined together and discretized in the explicit FDTD scheme, yielding

$$\boldsymbol{E}|^{n+1/2} = C_a\boldsymbol{E}|^{n-1/2} + C_b[\boldsymbol{\nabla}\times\boldsymbol{H}|^n - Re(\sum_{\boldsymbol{k=1}}^{\boldsymbol{L}}\frac{m}{2}(\mathbf{1} + \boldsymbol{k_p})\mathbf{J}_k|^{n-1/2})] \qquad (12)$$

$$\mathbf{J}_k|^{n+1/2} = \kappa_k\mathbf{J}_k|^{n-1/2} + \beta_k(\frac{\mathbf{E}|^{n+\frac{1}{2}} - \mathbf{E}|^{n-\frac{1}{2}}}{\Delta t}) \qquad (13)$$

Where

$$\begin{cases} C_a = \frac{2\varepsilon_0\varepsilon_\infty - \sigma\,\Delta t + Re\sum_{k=1}^{L}(m\beta_k)}{2\varepsilon_0\varepsilon_\infty + \sigma\,\Delta t + Re\sum_{k=1}^{L}(m\beta_k)}, \\ C_b = \frac{2\Delta t}{2\varepsilon_0\varepsilon_\infty + \sigma\,\Delta t + Re\sum_{k=1}^{L}(m\beta_k)} \\ \kappa_k = \frac{2 + p_k\Delta t}{2 - p_k\Delta t}\ ,\ \beta_k = \frac{2\varepsilon_0 r_k\Delta t}{2 - p_k\Delta t} \end{cases}$$

(m = 1, if p_k is real ; m = 2, if p_k is complex)

The discretization of the magnetic field $\boldsymbol{H}|^{n+1/2}$ is the same as it is in the standard FDTD algorithm [3].This is an efficient implementation of the general model in the FDTD method.

With the same number of poles, the general model takes no additional memory and computational costs for updating the auxiliary equations of the polarization currents compared with the conventional dispersion models such as multi-pole Lorentz-Drude model. However, the general model offers more degrees of freedom in fitting a permittivity function in the parameter estimation process. Thus, the implementation of the general model in the FDTD method is far more computationally efficient compared to those of Lorentz-Drude model. The general model is an analytical function that describes the relative permittivity of a dispersive material. To fit a given relative permittivity curve accurately and quickly, a parameter estimation procedure is highly demanded in obtaining a good initial guess for the starting point and locating a good approximation to the global optimum. The advantage of the fraction form of the general model in equation (1a) lies in the fact that a very good initial guess of parameters a_k and b_k can be quickly obtained using the rational approximation method [9].After that, the initial values of the residues r_k, poles p_k, and direct coefficient ε_∞ are obtained from the parameters a_k and b_k by converting the general model from the rational fraction form to the partial fraction form. Finally, the initial values are employed in a simulated annealing algorithm [5].to find the optimized values of parameters; ε_∞, $p_k$andr_k. The high efficiency of the general model is demonstrated in modeling metal materials Au (gold in a wide range of wavelength from 400 to 1100 nm). The measured relative permittivity of these three metals.is fitted using four dispersion models: the 4-pole Lorentz-Drude model (1 Drude pole pair and 1 Lorentz pole pair), the 6-pole Lorentz-Drude model (1 Drude pole pair and 2 Lorentz pole pairs), the general model with 4 poles, and the general model with 6 poles. The Lorentz-Drude model is expressed in the equation

$$\varepsilon_r(\omega) = \varepsilon_\infty + \frac{\omega_D^2}{-\omega^2 + j\omega\gamma_D} + \sum_{l=1}^{N_l} \frac{\Delta\varepsilon_l \omega_l^2}{-\omega^2 + 2j\omega\gamma_l + \omega_l^2} \quad (15)$$

Where, the numbers of Drude, and Lorentz pole pairs are one, and N_L respectively. As it is shown in Figure 1, both the Lorentz-Drude model and the general model achieve better accuracy with more number of poles. However, the general model overwhelms the Lorentz-Drude model with significant improvement of accuracy while having the same number of poles. Moreover, for some materials such as Au, the general model with 4 poles fits the experimental data to a higher accuracy than that of the 6-pole Lorentz-Drude model, while having much lower computational cost. The general model with 6 poles performs a much more accurate fit than the 6-pole Lorentz-Drude model, while having the same computational cost.black circles are experimental data taken from. the black dot and dash lines are fitting curves with 4-pole Lorentz-Drude model (1 Drude pole pair and 1 Lorentz pole pair) and 6-pole Lorentz-Drude model (1 Drude pole pair and 2 Lorentz pole pairs), respectively; the solid red and blue lines are the fitting curves with 4-pole and 6-pole general model, respectively.

To demonstrate the advantages of the general model in terms of the modeling accuracy, a convergence test of the general model is performed on the three metal materials Au. The convergence of the general model is studied by measuring the relative errors of the modeled permittivity with increasing the number of poles. The relative error of the modeled permittivity to the experimental data is defined by

$$e_{rel}(dB) = 5[log \sum_{i}^{N} |\varepsilon^{exp}(\omega_i) - \varepsilon(\omega_i)|^2 - log \sum_{i}^{N} |\varepsilon^{exp}(\omega_i)|^2] \quad (16)$$

Figure 2, depicts the relative errors of the general model and the Lorentz-Drude mode in modeling the permittivity of the metal materials Au. It shows that increasing the number of poles, both the general model and the Lorentz-Drude model reduce the relative error. However, the general model converges faster than the Lorentz-Drude model. The parameters of the Lorentz-Drude model and the general model for modeling material Au are listed in Table 2 and Table 3, respectively.

3. Numerical Simulations:

In this section, the general model is employed for modeling material properties of gold nanoparticles in the lightwave range with the FDTD method. It improves the accuracy of material modeling while does not increase the computing cost of the FDTD method. The optical properties such as absorption and extinction cross section and electric field enhancement of nano-ellipses are simulated by the accelerated 2D FDTD method and those of nano-ellipsoids are simulated by the accelerated 3D FDTD method. The parameters employed for modeling the gold material with the general model in the FDTD method are similar to what is listed in Table 3. 6 poles are used in the general model for all the simulations.

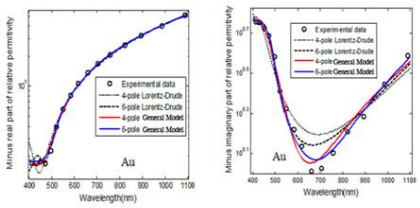

Fig. 1: (a) Real and (b) imaginary parts of the permittivity function of Au**.**

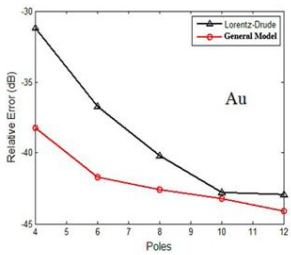

Fig. 2: Relative errors of modeled permittivity of Au.

Table 2: Values of the parameters for the Lorentz-Drude Model (Au).

Parameters	1 Drude 1 Lorentz	1 Drude 2 Lorentz	1 Drude 3 Lorentz	1 Drude 4 Lorentz	1 Drude 5 Lorentz
ε_∞	6.07	5.06	2.54	1.00	1.00
$\omega_D(eV)$	8.83	8.74	8.65	8.23	8.22
$\gamma_D(eV)$	5.62e-2	6.27e-2	6.60e-2	1.04e-7	3.54e-8
$\Delta\varepsilon_1$	1.93	7.36-1	8.83e-1	1.19	5.32e-1
$\omega_1(eV)$	3.04	2.75	3.08	3.09	2.68
$\gamma_1(eV)$	5.03e-1	2.86e-1	3.05e-1	3.87e-1	2.64e-1
$\Delta\varepsilon_2$	-	1.31	1.91	2.9	2.89
$\omega_2(eV)$	-	3.32	3.93	4.29	4.28
$\gamma_2(eV)$	-	3.49e-1	5.86e-9	1.28e-9	1.89e-7
$\Delta\varepsilon_3$	-	-	6.52e-1	5.29e-1	1.18
$\omega_3(eV)$	-	-	2.69	2.68	3.09
$\gamma_3(eV)$	-	-	-	2.63e-1	3.86e-1
$\Delta\varepsilon_4$	-	-	-	9.68	9.8
$\omega_4(eV)$	-	-	-	7.59	7.57e-1
$\gamma_4(eV)$	-	-	-	2.42	2.41e-1
$\Delta\varepsilon_5$	-	-	-	-	1.01e-6
$\omega_5(eV)$	-	-	-	-	2.74e-1
$\gamma_5(eV)$	-	-	-	-	8.01e-2

Table 3: Values of the parameters for the General Model (Au).

Parameters	4-pole General Model	6-pole General Model	Parameters	4-pole General Model	6-pole General Model
ε_∞	2.99	1.00	$p_4(eV)$	-6.81e-1-2.6i	-2.33e-1+2.52i
$p_1(eV)$	-1.75e-2 -1.08e-2i	-2.36e-2-8.55e-2i	$r_4(eV)$	3.7-1.67i	3.87e-1-3.14e-2i
$r_1(eV)$	1.46+3.4e+3i	1.53+402e+2	$p_5(eV)$	-	-1.19-2.39i
$p_2(eV)$	-1.75e-2+1.08e-2i	-2.35e-2+8.65e-2i	$r_5(eV)$	-	7.246+1.796e-1i
$r_2(eV)$	1.46-3.4e+3i	1.53-4.2e+2i	$p_6(eV)$	-	-1.186+2.390i
$p_3(eV)$	-6.8e-1-2.6i	-2.33e-1-2.52i	$r_6(eV)$	-	7.246-1.796e-1i
$r_3(eV)$	3.69+1.67i	3.87e-1+3.14e-2i			

3.1 Simulation of Nano-ellipsoid:

The simulation results of the optical scattering properties of a gold nano-ellipsoid with different radii surrounding by air are produced by the three-dimensional (3D) FDTD method combined with the general model. In the 3D FDTD simulation, a uniform mesh size of 1.0 nm is employed and 30,000 time steps are performed. In Figure 3,The absorption and extinction cross section spectraof Nano-ellipsoid with above four different configurations are compared and depicted. Figure3 shows that the absorption and extinction effect is enhanced by the volume of the nanoparticle.

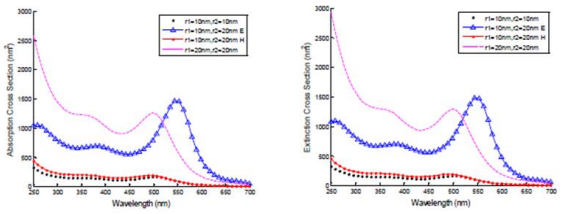

Fig. 3: absorption and extinction cross section spectraof gold nano-ellipsoids with different radii and incident wave polarizations**.**

3.2 Simulation of Nano-ellipse:

The optical properties such as the absorption and extinction cross section of a gold nano-ellipse with different configurations regarding the differences of sizes, incident wave angle and background materials are simulated using the 2D FDTD method accelerated by the high performanceGPU hardware with parallel computing technique. The TM polarization is used in the 2D FDTD simulations. The structure of the nano-ellipse is showed in Figure 4. It has a longer radius $r_2$and a shorter radiusr_1. The nano-ellipse is illuminated by an incident plane wave propagating toward it with an angle of alpha to the $r_2$axis.

The optical properties of this particle are studied in three cases. In the first case, the nano-ellipse with a longer radius $r_2 = 20\,nm$ and a shorter radius $r_1 = 10\,nm$ is surrounded by air. The plane wave propagates toward it from different directions, which means the angle alpha changes to different values. In the Figure 5, absorption and extinction cross section spectraincreases when angle alpha varying from 0 degree to 90 degree. It shows that the peak of the absorption and extinction cross section increases when angle size changes from 0 to 90 degrees. When

the longer axis of the nano-ellipse aligns with electric field polarization direction (alpha=90 degrees), the peaks reach the maximum. However, the peak positions in the spectra do not change in the simulations.

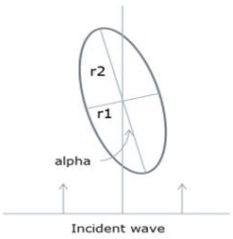

Fig. 4: Structure of a single nano-ellipse illuminated by an incident plane wave**.**

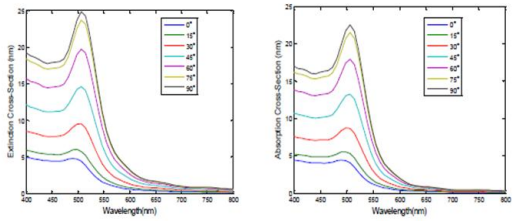

Fig. 5: Extinction and absorption cross section spectra of a nano-ellipse with incident wave illuminating from different directions.

In the second case, the nano-ellipse has the same size as that in the first case and the electric field of the incident wave is polarized to the direction in the radius axis (alpha=90 degrees). However, different surrounded materials such as air (index=1.0), water (index=1.33), silica (index=1.42), Polymethyl Methacrylate (index=1.49) and silicon (index=3.2) are used in the simulations. The extinction and absorption cross-sections are depicted in Figure 6. It shows that peaks of the cross-sections increase along with the increase of the background material refractive index. The only one exception is absorption spectrum when the particle issurrounded by silicon with refractive index as 3.2. Its peak is no larger than those of all the other spectra with lower surrounded material refractive indices. With the increase of the background refractive index, the peak positions in the spectra are shifted to the long wavelengths (red shift).

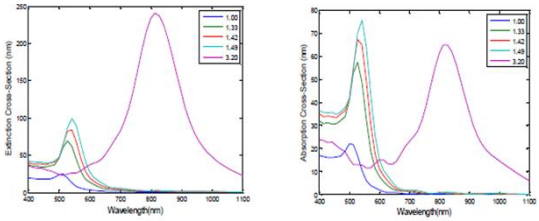

Fig. 6: Extinction and absorption cross-section spectra of a nano-ellipse surrounded by different materials.

The extinction and absorption cross-sections are depicted in Figure 7. It shows clearly that the peaks of the cross-sections increase with the increase of the radius size r2, but the peak positions are not sensitive.

3.3 Simulation of Nano-ellipse Dime:r

The optical properties of a gold nano-ellipse dimer shown in Figure 8 are simulated using the 2D FDTD method with TM polarization. The dimer consists of two identical nano-ellipses with a longer radius r2 and a shorter radius r1. The two nano-ellipses are aligned in the same axis of the radius r2. The incident plane wave propagates toward the dimer with an angle of alpha to the common axis. The distance between the nearest points on the two nanoellipses is d.

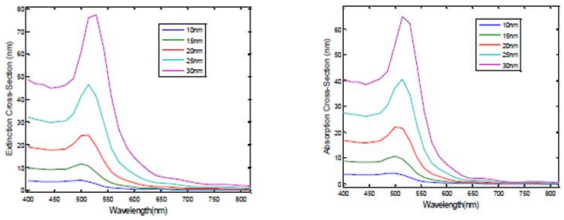

Fig. 7: Extinction and absorption cross-section spectra of a nano-ellipse with different raidus r2.

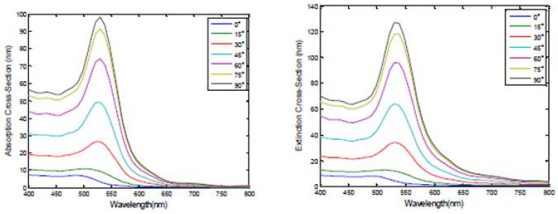

Fig. 8: Structure of a nano-ellipse dimer illuminated by an incident plane wave.

The optical properties of this nano-ellipse dimer are demonstrated in three cases. In the first case, the incident angle alpha is scanned from 0 degree to 90 degrees. The dimmer is surrounded by air with r1=10nm and r2=20nm. The distance between the two nano-ellipses is d=2nm. Figure 9, gives the extinction and absorption cross-section spectra for different incident angles. It shows that the peaks of the cross-section spectra keep increasing when alpha varies from 0 to 90 degrees but the peak positions do not change accordingly.

In the second case, the distance d between the two nano-ellipse in the dimer varies from 2nm to 6nm. The dimer is surrounded by air with r1=10nm and r2=20nm. Figure 10,shows the cross-section spectra for different values of d from 2nm to 6nm when the incident wave propagating along the common axis (alpha=0 degree)

The background refractive index of the dimer is changed to 1.00, 1.33, 1.42, 1.49 and 3.20 corresponding the materials air, water, silica, Polymethyl Methacrylate and silicon, respectively. The distance d is 2nm and the length of the radius r1 and r2 is 10nm and 20nm, respectively. The incident angle alpha=90 degrees. Figure 11, shows that with the increase of the background index, the peak of extinction crosssection spectrum increases and the peak position moves from the visible lightwave range to the infrared range.

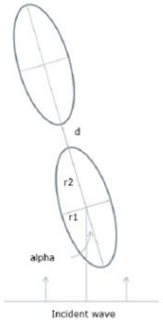

Fig. 9: Extinction and absorption cross-section spectra of a nano-ellipse dimer illuminated by incident wave from different angles**.**

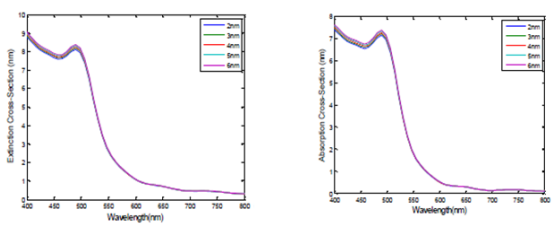

Fig. 10: Extinction and absorption cross section spectra of a nano-ellipse dimer with different values of distance between its two nano-ellipses. The angle alpha of the incident wave is 0 degree.

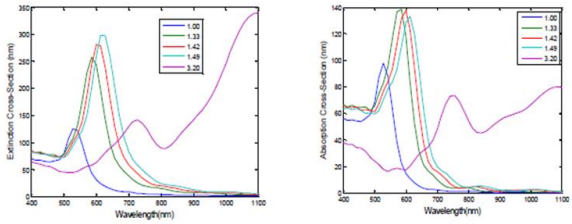

Fig. 11: Extinction and absorption cross-section spectra of a nano-ellipse dimer surrounded by different background materials. The angle alpha of the incident wave is 90 degrees.

Table 4, lists the memory and computational costs of different FDTD schemes, as well as the relative errors of the extinction cross-section compared with the analytical solution. It shows that compared with the conventional Lorentz-Drude model, the FDTD method with the 4-pole General Model achieves a smaller relative error while taking much less computational effort, and the FDTD method with the 6-pole achieves even better accuracy yet maintaining a comparable computational cost. It proves that the general model is more efficient in terms of memory and computational costs in modeling dispersive materials in comparison with conventional models. It is a powerful and efficient tool for simulating broadband optical phenomena of nanoparticles with dispersive materials.

Table 4: Computational costs and relative errors of different FDTD schemes.

	Scheme 1 (1 Drude pole pair and 2 Lorentz pole pairs)	Scheme 2 (4 General Model poles)	Scheme 3 (6 General Model poles)
Memory (mega-byte)	6.600	5.872	6.604
Computation time (second)	694.58	599.26	702.04
Relative error (dB) (Extinction cross section	-23.97	-25.31	-26.04

4. Conclusion:

The optical properties of a single gold nano-ellipsoid are simulated by the 3D FDTD method first. The general model is employed for modeling the susceptibility of the dispersive material. It shows that the absorption effect of a gold single nano-ellipsoid is mainly affected by the length of the radius which is parallel to the direction of theelectric field polarization. A single gold nano-ellips, a gold nano-ellipse dimerare simulated with the 2D FDTD method with general model for modeling the material susceptibility. The extinction absorption cross-section spectra of them are studied in many cases where the incident wave angle, the value of d, the length of the radius r2 and the refractive index of the background material is changed, respectively. The cross-section spectra of a nano-ellipse dimer are much more sensitive to the change of the distance d in the situation where the electric field polarization is parallel to the common axis than that in the situation where the electric field polarization is perpendicular to the common axis. This systematic study of the optical properties of different nano-particles gives a good reference for design of optical devices utilizing the cross-section spectra characteristics of nano-particles, such as optical sensors, optical filters, heat sinks, etc.

References

1. Akbar Asadi, and Ahmad Mohammadi, 2014. FDTD Formulation for The General Dispersion Model Using the Z Transform Method. MathematicaAeterna, 4(4): 411– 424.
2. Chang, S.H., S.K. Gray, G.C. Schatz, 2005. Surface plasmon generation and light transmission by isolated nanoholes and arrays of nanoholes in thin metal films. Optics Express, 13(8), 3150. doi:10.1364/opex.13.003150.
3. Hamidi, M., 2011. Implementation of the critical points model in a SFM-FDTD code working in oblique incidence. Journal of Physics D: Applied Physics, 44: 245101.
4. Hao, F., P. Nordlander, 2007. Efficient dielectric function for FDTD simulation of the optical properties of silver and gold nanoparticles. Chemical Physics Letters, 446(1-3): 115–118. doi:10.1016/j.cplett.2007.08.027.
5. Kirkpatrick, S., C.D. Gelatt, M.P. Vecchi, 1983. Optimization by Simulated Annealing. Science, 220(4598), 671–680. doi:10.1126/science.220.4598.671

6. Minghui Han, Dutton, R.W. Shanhui Fan, 2006. Model dispersive media in finite-difference time-domain method with complex-conjugate pole-residue pairs. IEEE Microw. Wireless Compon. Lett., 16(3): 119–121. doi:10.1109/lmwc.2006.869862.
7. Rakic, A.D., A.B. Djurišic, J.M. Elazar, M.L. Majewski, 1998. Optical Properties of Metallic Films for Vertical-Cavity Optoelectronic Devices. Appl. Opt., 37(22): 5271. doi:10.1364/ao.37.005271.
8. Taflove, A., S.C. Hagness, 2005. Finite-Difference Time-Domain Analysis. Encyclopedia of RF and Microwave Engineering. doi:10.1002/0471654507.eme123.
9. Ubolli, A., B. Gustavsen, 2011. Comparison of Methods for Rational Approximation of Simulated Time-Domain Responses: ARMA, ZD-VF, and TD-VF. IEEE Transactions on Power Delivery, 26(1): 279–288. doi:10.1109/tpwrd.2010.2080361
10. Udagedara, I., M. Premaratne, I.D. Rukhlenko, H.T. Hatori, G.P. Agrawal, 2009. Unified perfectly matched layer for finite-difference time-domain modeling of dispersive optical materials. Optics Express, 17(23): 21179. doi:10.1364/oe.17.021179.
11. VahidNayyeri, Mohammad Soleimani, and Omar M. Ramahi, *2013.* Wideband Modeling of Graphene Using the Finite-Difference Time-Domain Method, IEEE trans, on antennas and propagations, 61-12.
12. Vial, A., T. Laroche, 2008. Comparison of gold and silver dispersion laws suitable for FDTD simulations. Applied Physics B, 93(1), 139–143. doi:10.1007/s00340-008-3202-4.
13. Vial, A., A.S. Grimault, D. Macías, D. Barchiesi, M. de la Chapelle, 2005. Improved analytical fit of gold dispersion: Application to the modeling of extinction spectra with a finite-difference time-domain method. Phys. Rev. B, 71(8). doi:10.1103/physrevb.71.085416.